Available online at www.sciencedirect.com
ScienceDirect
Journal of Catalysis 254 (2008) 27–38
JOURNAL OF CATALYSIS
www.elsevier.com/locate/jcat

Methane dissociative chemisorption on Ru(0001) and comparison to metal nanocatalysts

Heather L. Abbott, Ian Harrison *

Department of Chemistry, University of Virginia, Charlottesville, VA 22904-4319, USA

Received 29 September 2007; revised 5 November 2007; accepted 10 November 2007

Abstract

Microcanonical unimolecular rate theory (MURT) was used to characterize methane dissociative chemisorption on Ru(0001). Simulations of supersonic molecular beam and thermal bulb-derived dissociative sticking coefficients indicated that the threshold energy for CH_4 dissociative chemisorption on Ru(0001) was $E_0 = 59$ kJ/mol and that two surface oscillators were active in the gas-surface collision complexes. MURT analysis of CH_4 supersonic beam experiments on several surfaces found that E_0 decreased from Ni(100) → Ru(0001) → Pt(111) → Ir(111). Although MURT simulations of CH_4 thermal dissociative sticking coefficients were in fairly good accord with thermal bulb experiments at mbar pressures, they were as much as 3–4 orders of magnitude higher than the apparent sticking coefficients derived from CH_4 decomposition or reforming rates on supported nanoscale metal catalysts. Consequently, the varied surface science studies on single crystals all strongly suggested that relatively few surface sites were turning over on the CH_4-reforming nanocatalysts.

Keywords: Ruthenium; Alkane; C–H activation; Molecular beams; Catalysis; Reforming; Reaction dynamics; Kinetics; Transition state theory

1. Introduction

Energy concerns have heightened interest in optimizing heterogeneously catalyzed alkane-reforming reactions that produce hydrogen. In particular, the industrial importance of steam reforming of natural gas, a process in which CH_4 and H_2O are reacted over a Ni catalyst to produce synthesis gas, a mixture of H_2 and CO, has encouraged researchers to seek more insight into methane dissociative chemisorption on metal surfaces. Recent studies [1–6] of the high-temperature decomposition and reforming of methane on supported metal nanocatalysts indicate that the initial C–H bond breaking of CH_4 is the rate-determining step. Although the threshold energy for CH_4 bond dissociation decreases from 432 kJ/mol in the gas phase [7] to only 65 kJ/mol on a Ni(100) surface [8,9], surfaces with even lower threshold energies for dissociative chemisorption might be better catalysts if catalytic turnover can be maintained and coking avoided. Ultra-high-vacuum (UHV) surface science experiments have examined methane dissociative chemisorption on a number of potentially useful metals for methane reforming (e.g., Ni(100) [10–16], Pt(111) [17–20], Pd(111) [21,22], Ir(111) [23,24], Rh(111) [25,26], and Ru(0001) [27–30]), often using nonequilibrium molecular beam techniques [31]. In this work, microcanonical unimolecular rate theory (MURT) was used to extract transition state characteristics for CH_4/Ru(0001) dissociative chemisorption through an analysis of dissociative sticking experiments using supersonic molecular beam and thermal bulb methods. The dynamics of methane activation are discussed in the context of the MURT and an alternative, reduced-dimensionality, dynamic approach based on vibrationally resolved dissociative sticking coefficients obeying an error function form. Based primarily on the analysis of supersonic molecular beam experiments, MURT simulations of CH_4 thermal dissociative sticking coefficients, S_T, on several metal surfaces are calculated to be 2–4 orders of magnitude higher than apparent S_T values derived from turnover rates for CH_4 reforming on metal nanocatalysts.

The dissociative chemisorption of methane on ruthenium surfaces has been examined by both surface science [27–30] and catalysis [3,32] techniques. Wu and Goodman [28] mea-

* Corresponding author.
E-mail address: harrison@virginia.edu (I. Harrison).

0021-9517/$ – see front matter
doi:10.1016/j.jcat.2007.11.013

sured S_T for CH_4 on Ru(0001) at a pressure of ~7 mbar. An activation energy of $E_a = 36$ kJ/mol was derived from an Arrhenius fit of S_T over the experimental temperature range of $500 \leqslant T \leqslant 650$ K. Later measurements of S_T by Egeberg et al. [27] using a thermal bulb technique at ~5 mbar pressure, were within an order of magnitude of the values reported by Wu and Goodman [28], but the activation energy of $E_a = 51 \pm 6$ kJ/mol was 15 kJ/mol higher. Step-blocking experiments found that step sites are not discernibly more reactive than terrace sites for methane dissociative chemisorption on Ru(0001) [27], unlike the case for N_2 dissociative chemisorption [33,34].

Catalysis experiments [3,32] characterizing the dissociative chemisorption of methane over oxide-supported ruthenium nanoparticles yielded apparent sticking coefficients 10^2–10^3 times lower than those reported by Wu and Goodman [28] and Egeberg et al. [27] for CH_4/Ru(0001). Carsten and Bell [32] measured an activation energy of $E_a = 27 \pm 2$ kJ/mol for dissociative sticking of CH_4 on 6-nm average diameter Ru particles on SiO_2 over the temperature range $473 \leqslant T \leqslant 673$ K, whereas Wei and Iglesia [3] measured $E_a = 99$ kJ/mol for 3-nm average diameter Ru particles on Al_2O_3 for $823 \leqslant T \leqslant 1023$ K. Kinetic and isotopic tracer and exchange experiments performed by Wei and Iglesia [3] at the higher temperatures found that CH_4 decomposition and reforming rates on Ru nanoparticles are virtually identical, structure-sensitive, independent of the oxide support composition, and rate-limited by the initial C–H bond cleavage of CH_4.

Nonequilibrium supersonic molecular beam studies by Larsen et al. [29] explored the roles of translational and vibrational energy in the dissociation of methane on Ru(0001). The dissociative sticking coefficient S was found to scale with the normal translational energy $E_n = E_t \cos^2 \vartheta$, where E_t is the molecular translational energy and ϑ is the angle between the incident molecules and the surface normal. By varying the nozzle temperature T_n, angle of incidence ϑ, and the seeding mixture of the methane gas, Larsen et al. [29] changed the normal translational energy of the supersonic molecular beam and observed that S increased with E_n. In these experiments, S was also found to increase with increasing nozzle temperature, and hence with increasing molecular vibrational temperature T_v, which is fixed by T_n (i.e., $T_v = T_n$). The role of rotational energy was not probed in these supersonic molecular beam experiments because of efficient collision-induced cooling of methane rotations (i.e., $T_r \sim 0.1 T_n$) during the supersonic expansion [10]. Larsen et al. [29] optimized a nine-parameter empirical error function (erf) model to fit their molecular beam sticking data and then simulated S_T. An Arrhenius fit to this S_T gave an activation energy of $E_a = 37$ kJ/mol.

A further supersonic molecular beam study of methane/Ru(0001) reactivity by Mortensen et al. [30] examined surface temperature and isotope effects. Dissociative sticking was found to increase with increasing surface temperature T_s. The dependence of S on T_s became more pronounced as E_n was diminished (i.e., $\partial S/\partial T_s$ increased as E_n decreased). A remarkably high kinetic isotope effect of ~20 was found by comparing S for CH_4 and CD_4 [30]. Mortensen et al. [30] adapted the erf model used by Larsen et al. [10] by incorporating a surface temperature dependence into one of the adjustable parameters and used this updated erf model to successfully fit their supersonic molecular beam data [30], as well as the thermal equilibrium and nonequilibrium (i.e., $T_g = 300$ K; $T_g \neq T_s$) bulb data of Larsen et al. [10].

Electronic structure calculations have been performed using periodic generalized gradient approximation–density functional theory (GGA–DFT) for methane decomposition on ruthenium. GGA–DFT computations by Ciobica et al. [35] found a threshold energy for the initial C–H bond cleavage of methane on Ru(0001) of $E_0 = 85$ kJ/mol. However, the most energy-demanding step along the pathway to complete decomposition of methane is the last one, requiring a calculated $E_0 = 108$ kJ/mol to break the C–H bond of chemisorbed methylidyne (i.e., $CH_{(c)} \rightarrow C_{(c)} + H_{(c)}$). Similar GGA–DFT calculations by Liu and Hu [36] found a somewhat lower threshold energy of $E_0 = 76$ kJ/mol for the initial C–H bond cleavage of CH_4 on Ru(0001) terrace sites, but also found that step and kink sites were more reactive with an E_0 about 30 kJ/mol lower. Using cluster unity bond index–quadratic exponential potential (UBI–QEP) methods, Au et al. [37] calculated an activation energy of $E_a = 60$ kJ/mol for an initial C–H bond cleavage of CH_4 on a 10-atom ruthenium cluster, the lowest activation energy computed for this process on any of the transition metals that they investigated (i.e., Os, Rh, Ir, Pd, Cu, Ag, and Au). Au et al. [37] also calculated that methylidyne dissociation with $E_a = 115$ kJ/mol had the highest activation energy of any of the methane decomposition steps. Other UBI–QEP calculations by Lin et al. [38] gave an activation energy of $E_a = 47$ kJ/mol for the initial C–H bond cleavage of CH_4 on Ru(0001), which was lower than values obtained on the other transition metal surfaces that they considered (i.e., Pt(111), Rh(111), Ir(111), Ni(111), and Cu(111)). Unfortunately, these varied electronic structure theory calculations do not consistently identify a common activation energy for the first C–H bond cleavage of methane on Ru(0001), nor do they identify the rate-determining step for methane decomposition. The substantial entropy reduction occurring as gas-phase methane accesses the transition state for the initial C–H bond cleavage means that the dissociation rate constant or dissociative sticking coefficient for this step could have a particularly low pre-exponential factor [39], thereby theoretically allowing this step to compete against methylidyne decomposition as the rate-determining step in methane decomposition despite the unfavorable difference in the calculated activation energies. In CH_4 reforming, where oxygen will be available on the surface, the GGA–DFT computed barriers [40] for oxidation of methylidyne on Ni(111) to form CHO and its subsequent decomposition to CO + H are much lower than those for methylidyne decomposition, arguing for a rate-limiting function of the initial C–H bond cleavage of CH_4.

In summary, a range of E_a values for the initial C–H bond cleavage of methane on Ru(0001) from 47–85 kJ/mol have been proposed theoretically, and values from 27–99 kJ/mol have been extracted from experiments. As a transition state theory applicable to activated dissociative chemisorption under both nonequilibrium and equilibrium conditions, MURT

affords an opportunity to extract relatively robust transition state parameters defined by their ability to optimally simulate as diverse a range of experiments as possible. MURT has been applied previously to model alkane dissociative chemisorption of relevance to reforming (i.e., CH_4 on Pt(111) [20,41,42], Ni(100) [8,9,43], and Ir(111) [44]; C_2H_6 on Pt(111) [45]), the dissociative chemisorption and recombinative desorption dynamics of H_2 on Cu(111) [46,47] and CO_2 on Rh(111) [48], and the dissociative chemisorption of SiH_4 on Si(100) [49]. Typically, a three-parameter formulation of the MURT is able to reproduce experimental data with an average relative discrepancy of about 50%, even for quantum state-resolved sticking measurements [8,47,48]. Unfortunately, in the present work, only semiquantitative agreement between the 3-parameter MURT simulations and the available experimental data for methane/Ru(0001) dissociative chemisorption was achieved, and the 9-parameter semiempirical erf model was found to simulate the experiments somewhat better. Nevertheless, MURT analysis of diverse experiments allows for a theoretically rigorous characterization of the CH_4/Ru(0001) transition state and thereby allows comparisons to CH_4 reactivity on other surfaces and under other experimental conditions. Here we contrast MURT simulations of CH_4 thermal dissociative sticking coefficients on Ru(0001), Pt(111), Ni(100), and Ir(111) based on MURT analysis of supersonic molecular beam experiments and compare these results with those derived from thermal bulb experiments and thermal decomposition rates for CH_4 on nanocatalysts operating at ∼1 bar pressure. Periodic trends in reactivity are identified, and the thermal dissociative sticking coefficients are calculated to be three to four orders of magnitude higher on single crystal surfaces compared with apparent values for the nanocatalysts. The simplest explanation for this discrepancy is to speculate that only relatively few surface sites on the nanocatalysts are able to repetitively turn over under high-pressure catalytic conditions.

2. Physisorbed complex–microcanonical unimolecular rate theory

The microcanonical unimolecular rate theory (MURT) is schematically depicted in Fig. 1 and has been described in detail elsewhere [9,41,42]. Briefly, the MURT presumes that an incident molecule interacts locally with only a few surface oscillators/atoms to form a transient collision complex or a physisorbed complex (PC). The energy of a PC is assumed to be quickly randomized by the initial collision dynamics and/or by rapid intramolecular vibrational energy redistribution in an ensemble averaged sense such that all states at a particular energy E^* become equally probable. For small molecules with desorption lifetimes on the surface that are ultrafast at the reactive energies of interest (e.g., $\tau_D \sim 2$ ps for CH_4 on Ni(100)) [9], master equation calculations with realistic energy transfer rates to the surrounding substrate [41,42,44] indicate that the PCs are approximately adiabatically isolated over their lifetime. Consequently, the PC–MURT reaction kinetics for activated dissociative chemisorption can be written as

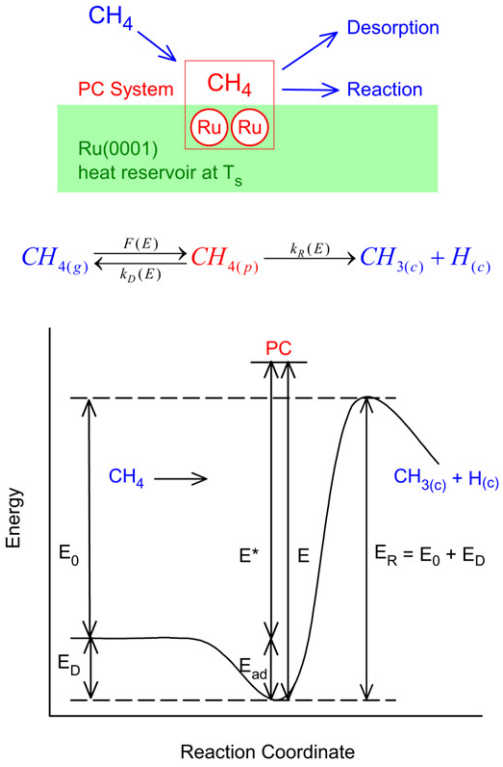

Fig. 1. A schematic depiction of the PC–MURT kinetics is shown with zero point energies implicitly included in the 2D potential energy curve and the surface degrees of freedom suppressed for clarity.

$$\mathrm{CH_{4(g)}} \underset{k_D(E^*)}{\overset{F(E^*)}{\rightleftarrows}} \mathrm{CH_{4(p)}} \overset{k_R(E^*)}{\rightarrow} \mathrm{CH_{3(c)}} + \mathrm{H_{(c)}}, \tag{1}$$

where $F(E^*)$ is the flux distribution for PC formation; $k_D(E^*)$ and $k_R(E^*)$ are Rice–Ramsperger–Kassel–Marcus (RRKM) energy-dependent rate constants [50,51] for desorption and reaction, respectively; and the surface coordination numbers have been suppressed. Application of the steady-state approximation to the coverage of PCs (i.e., $CH_{4(p)}$ in Eq. (1)) yields the experimentally observable sticking coefficient

$$S = \int_0^\infty S(E^*) f(E^*)\, dE^*, \tag{2}$$

where

$$S(E^*) = \frac{W_R^\ddagger(E^* - E_0)}{W_R^\ddagger(E^* - E_0) + W_D^\ddagger(E^*)} \tag{3}$$

is the microcanonical sticking coefficient; $W_D^\ddagger$ and $W_R^\ddagger$ are the sums of states at the transition states for desorption and reaction, respectively; E_0 is the threshold energy for dissociative chemisorption; and

$$f(E^*) = \int_0^{E^*} f_n(E_n) \int_0^{E^*-E_n} f_v(E_v) \int_0^{E^*-E_n-E_v} f_r(E_r) \times f_s(E^* - E_n - E_v - E_r)\, dE_r\, dE_v\, dE_n \tag{4}$$

is the flux distribution for creating a PC with total exchangeable energy $E^* = E_n + E_v + E_r + E_s$. The $f(E^*)$ is formed

by convolution over the flux-weighted molecular (i.e., normal translational, vibrational, and rotational) and surface energy distributions. The E^* energy floor is taken to occur when methane is freely rotating and vibrating far from the surface at $T = 0$ K. Molecular beam experiments [30] have shown that the methane/Ru(0001) initial dissociative sticking coefficient scales with only the normal translational energy. Consequently, parallel translational energy $E_p = E_t \sin^2 \vartheta$ is treated as a spectator to the dissociation dynamics. This is consistent with the effective conservation of parallel momentum until after dissociation and provides some indication that the gas-surface interaction potential is relatively smooth and uncorrugated across the plane of the surface. Following standard practice for supersonic molecular beams of methane [31], the nozzle temperature is assumed to set the vibrational and rotational temperatures as $T_v = T_n$ and $T_r = 0.1T_n$, respectively, and the translational temperature of the beam is assumed to be $T_t \sim 25$ K. The $f(E^*)$ distribution for creating a PC at energy E^* is fixed by the experimental conditions (e.g., T_n and T_s), but the microcanonical sticking coefficient depends on the desorption and reaction transition states. The desorption transition state is taken to occur when the incident molecule is freely rotating and vibrating in the gas phase infinitely far from the surface. The reactive transition state for dissociative chemisorption is characterized in part by assuming the gas-phase methane vibrational mode frequencies are retained, the ruthenium surface atoms vibrate at the mean phonon frequency of bulk Ru (i.e., $\nu_s = (3/4)k_B\Theta_D/h = 310$ cm^{-1}, where k_B is the Boltzmann constant and Θ_D is the Debye temperature for Ru), and the ν_3 asymmetric C–H stretching vibration is the reaction coordinate. Three adjustable parameters are introduced to complete the characterization of the reactive transition state: (i) E_0, the reaction threshold energy for dissociative chemisorption; (ii) s, the number of surface oscillators participating in the PC; and (iii) ν_D, a grouped mean frequency representative of the three frustrated rotations and the vibration of methane along the surface normal at the transition state. These parameters were determined by minimizing the average relative discrepancy (ARD) between PC–MURT simulations and the available experimental data. The ARD is defined as

$$\mathrm{ARD} = \left\langle \frac{|S_{\mathrm{theory}} - S_{\mathrm{expt}}|}{\min(S_{\mathrm{theory}}, S_{\mathrm{expt}})} \right\rangle, \tag{5}$$

where S is the experimental parameter of interest (e.g., the dissociative sticking coefficient). Simulation of all of the available surface science experimental data for CH_4 dissociative sticking on Ru(0001) yielded an optimal parameter set of ($E_0 = 59$ kJ/mol, $s = 2$, and $\nu_D = 155$ cm^{-1}), which gave an overall ARD of 316%.

PC–MURT calculations were performed with Mathematica software on a personal computer using well-established RRKM algorithms that are widely applied to unimolecular reactions of polyatomic molecules in the gas-phase [50,51]. PC–MURT is a rigorous, full-dimensional, microcanonical transition state theory (TST) developed to treat activated gas-surface reactions subject to the approximation that ultrafast desorption rates at reactive energies (i.e., $E^* \geqslant E_0$) limits energy exchange between the transiently formed PCs and their surroundings. PC–MURT treats nonequilibrium and thermal equilibrium dissociative sticking on an equal footing through common application of Eq. (2). For experiments performed under thermal equilibrium conditions, PC–MURT recovers canonical TST and Arrhenius rate constants. Importantly, PC–MURT provides an opportunity to close the "nonequilibrium gap" that can make it difficult to compare the results of nonequilibrium surface science experiments with (i) electronic structure theory (EST) calculations of transition state characteristics and (ii) the results of thermal equilibrium catalysis experiments. For example, the 3 transition state parameters required by PC–MURT can be extracted from analysis of varied nonequilibrium surface science experiments, allowing for comparison to EST calculations, and the thermal dissociative sticking coefficient can be simulated by Eq. (2) for comparison to high-pressure thermal catalysis experiments. In this work, PC–MURT was applied to analyze all of the available nonequilibrium and thermal equilibrium dissociative sticking data for CH_4/Ru(0001) to extract as robust a set of transition state parameters as possible.

3. Results and discussion

3.1. PC–MURT analysis of dissociative sticking coefficients

Experimentally derived dissociative sticking coefficients for methane on Ru(0001) and on oxide-supported ruthenium nanoparticles are compared with methane/Ru(0001) PC–MURT simulations in Fig. 2. Although the optimal transition state parameter set gave the lowest overall ARD of 316%, alternative parameter sets were better able to describe restricted sets of experiments. For instance, ($E_0 = 71$ kJ/mol, $s = 2$, and $\nu_D = 85$ cm^{-1}) describes the supersonic molecular beam experiments [30] of Figs. 2a and 2b with an ARD = 42%, and ($E_0 = 54$ kJ/mol, $s = 1$, and $\nu_D = 495$ cm^{-1}) yields an ARD = 34% for the thermal equilibrium experiments [27,28] of Fig. 2d. Nevertheless, these alternative parameter sets failed to capture the general curvature of the remaining experimental S values as well as the optimal parameter set and generated higher ARDs for the complete set of S data. The qualitative agreement between the experimental sticking and the PC–MURT calculations suggests that a statistical description captures the essential features of the reaction dynamics, despite the relatively large ARD.

Fig. 2a shows how S increases with increasing E_n for both CH_4 and CD_4. PC–MURT reproduces the order of magnitude of the experimental S, but predicts a shallower slope $\partial S/\partial E_n$ than is observed experimentally (ARD = 18%). Fig. 2a also illustrates the large kinetic isotope effect (KIE) observed for methane dissociation on Ru(0001). Mortensen et al. [30] reported a KIE ~20 and suggested that classical effects, including the zero point energy correction of the reaction threshold energy E_0 and frequency shifts of the transition state vibrations, were responsible. PC–MURT incorporates these primary isotope effects, but predicts a KIE of only 3.6 for Mortensen et al.'s supersonic molecular beam experiments [30]. Similar supersonic molecular beam experiments examining methane dissociative

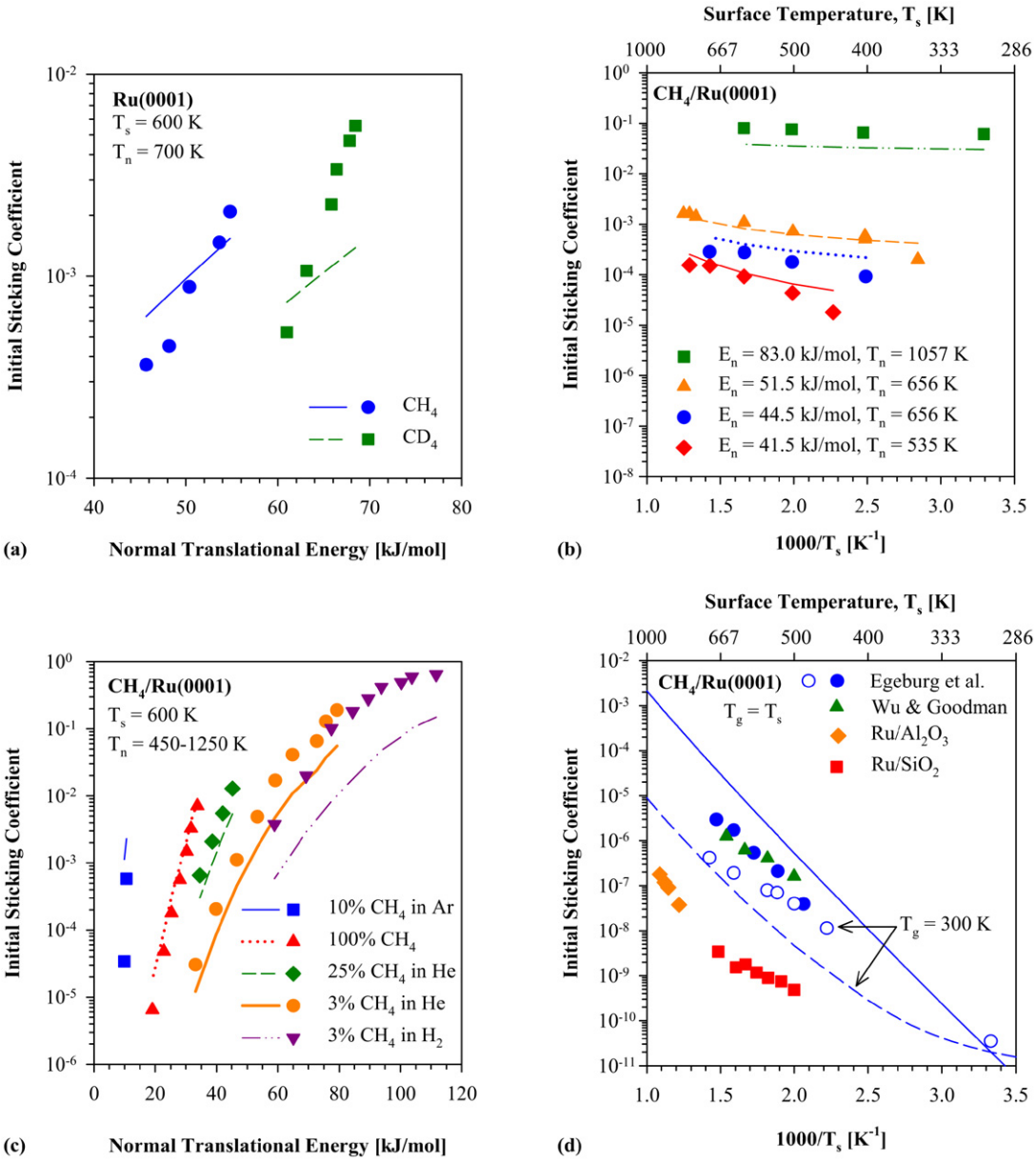

Fig. 2. Dissociative sticking coefficients, S, for methane on Ru(0001) derived from experiments (points) are compared to PC–MURT simulations. The overall average relative discrepancy (ARD) between experiments and theory is 316%. Supersonic molecular beam derived [30] S as a function of: (a) E_n yields an ARD = 102%; (b) T_s yields an ARD = 63%; (c) E_n and T_n for various seeding mixtures at $T_s = 600$ K yields an ARD = 401%. (d) Thermal bulb derived S_T for ambient CH_4 gas randomly impinging on Ru(0001) [27,28] and Ru nanocatalyst [3,32] surfaces. Open points and dashed lines are for S at variable T_s under an ambient CH_4 gas at $T_g = 300$ K. The ARD for the Ru(0001) thermal bulb data is 617%.

chemisorption on Pt(111) [17] and Ni(100) [10] reported KIEs of ∼3 and 5–10, respectively. Kinetic isotope effects of 3–4 and ∼4.5 have been measured under other nonequilibrium conditions (i.e., $T_g = 300$ K and variable T_s) by Mullins et al. [23] on Ir(111) and by Winters [52] on a tungsten filament, respectively. Wei and Iglesia measured kinetic isotope effects of 1.51, 1.58, 1.71, 1.68, and 1.60 for thermal decomposition of CH_4 on Ru [3], Pt [1], Ni [4], Ir [5,6], and Rh [2] nanoparticles, respectively. Thus, the KIE of ∼20 observed by Mortensen et al. [30] for methane/Ru(0001) is unusually high.

Mortensen et al. [30] examined the role of surface temperature on the CH_4/Ru(0001) dissociative sticking as shown in Fig. 2b for several normal translational energies. As the normal translational energy decreases from $E_n = 83.0$ to 41.5 kJ/mol, the slope of the sticking coefficients with respect to the surface temperature becomes steeper (i.e., $\partial S/\partial T_s$ increases). This is consistent with the surface degrees of freedom acting as a flexible energy reservoir that can contribute more energy to aid in surmounting E_0 when insufficient energy is available from the molecular degrees of freedom. Fig. 2d shows similar behavior for $S(T_s; T_g = 300$ K) as T_s increases, and also for S in CH_4 molecular beam studies on Pt(111) [18,20], Ni(100) [10], and Ir(111) [23].

The S determined by Larsen et al.'s [29] supersonic molecular beam experiments are displayed in Fig. 2c. The relatively poor agreement between the PC–MURT and Larsen et al.'s S

data [29] is somewhat surprising, because the model has successfully reproduced [8,9,43] similar data for CH_4 dissociation on Ni(100) obtained from the same laboratory [10].

Fig. 2d compares nonequilibrium [27] $S(T_s; T_g = 300\ \mathrm{K})$ and thermal equilibrium [27,28] S_T dissociative sticking coefficients measured in thermal bulb experiments for CH_4 on Ru(0001) with PC–MURT simulations. The figure also displays apparent S_T values for CH_4 dissociative chemisorption on Ru nanocatalysts determined by higher-pressure catalysis experiments [3,32]. The PC–MURT bounds the CH_4/Ru(0001) experimental data and captures the essential curvature of the methane dissociative sticking curves, but does not quantitatively represent the data very well with an ARD = 617%. Overlap between the $S(T_s; T_g = 300\ \mathrm{K})$ and S_T experimental data near $T_s \sim 500$ K suggests that the nonequilibrium experimental sticking at low T_s may be slightly high. Certainly, the surface is able to play a major role in activating CH_4, as evidenced by the 4 order of magnitude change observed in $S(T_s; T_g = 300\ \mathrm{K})$ with variation only in surface temperature. The apparent S_T values measured on the nanocatalysts are two to three orders of magnitude lower than those observed on Ru(0001) and lower still compared with the PC–MURT simulation. This discrepancy is intriguing because the high-curvature nanocatalyst particles expose an increased number of the presumably more reactive step and kink sites compared with Ru(0001), and the reactivity of the supported nanocatalysts increases by as much as a factor of five as particle size decreases [3].

Typically, methane dissociative sticking coefficients on metal surfaces have been determined by measuring the remaining carbon coverage using Auger electron spectroscopy (AES). But AES is not viable for carbon detection on Ru(0001), because the carbon and ruthenium AES peaks overlap. Instead, temperature-programmed oxidation (TPO) and/or high-resolution electron energy loss spectroscopy (HREELS) were used to monitor methane dissociation in the surface science experiments discussed above. Calibration of these methods to determine absolute sticking coefficients may be more challenging than for AES, which may explain some of the unusual difficulty encountered when using PC–MURT to simulate the varied dissociative sticking results obtained from different surface science laboratories and techniques.

PC–MURT is able to semiquantitatively simulate S for CH_4/Ru(0001) over a wide dynamic range with a reaction threshold energy of $E_0 = 59$ kJ/mol. Activation energies, obtained by experimental measurements as well as theoretical methods, have been depicted as a function of publication year in Fig. 3. The PC–MURT reaction threshold energy $E_0 = 59$ kJ/mol and activation energy at $T = 600$ K E_a (600 K) = 66 kJ/mol are intermediate within the range of computationally determined [35–38,53] (i.e., $E_0 = 47$–85 kJ/mol) and experimentally derived [3,27–30,32] (i.e., $E_a = 25$–99 kJ/mol) values. The PC–MURT value of $E_0 = 59$ kJ/mol agrees well with Au et al.'s unity bond index-quadratic exponential potential (UBI–QEP) [38] value of $E_0 = 60$ kJ/mol, whereas the PC–MURT E_a (600 K) = 66 kJ/mol is somewhat high compared with Egeberg et al.'s experimental value of $E_a = 51 \pm 6$ kJ/mol [27]. Interestingly, thermal experiments conducted

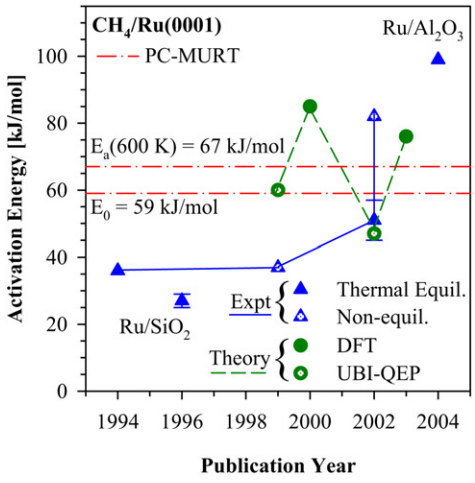

Fig. 3. Activation energies E_a and reaction threshold energies E_0 ($= E_a(0\ \mathrm{K})$) are shown as a function of publication year. Experimental thermal equilibrium E_as were obtained by performing Arrhenius fits to S_T data [3,27,28,32], while nonequilibrium E_as were derived from calculations of S_T based on an error function model fitted to nonequilibrium supersonic molecular beam data [29,30]. PC–MURT, density functional theory (DFT) [35,36,53], and unity bond index–quadratic exponential potential (UBI–QEP) [37,38] values for E_0 are also given.

on nanocatalyst particles gave the lowest and highest experimental activation energies (i.e., $E_a = 27 \pm 2$ and 99 kJ/mol). These nanocatalyst particles were deposited on SiO_2 [32] and Al_2O_3 [3] substrates with diameters of approximately 6 and 3 nm, respectively.

3.2. Comparison to the semiempirical error function model

Molecular beam dissociative sticking coefficients for methane have often been analyzed using a semiempirical error function form [54],

$$S_\nu(E_n) = \frac{A(\upsilon)}{2}\left[1 + \mathrm{erf}\left(\frac{E_n - \bar{E}_d(\upsilon)}{W(\upsilon, T_s)}\right)\right], \tag{6}$$

for the dissociative sticking coefficient $S_\nu(E_n)$ of the νth molecular vibrational mode in which $A(\upsilon)$, $\bar{E}_d(\upsilon)$, and $W(\upsilon, T_s)$ are adjustable parameters. The $S_\nu(E_n)$ has a sigmoid shape as a function of E_n. The $A(\upsilon)$ parameter gives the limiting value of the sticking coefficient at high E_n, $\bar{E}_d(\upsilon)$ is the value of E_n at the inflection point when the sticking has reached half of its limiting value, and $W(\upsilon, T_s)$ is a width parameter which dictates the slope of the curve around its inflection point. Although there is no rigorous theoretical derivation relating Eq. (6) to experimental dissociative sticking coefficients, one motivation for the erf model is to assume that incident molecules dynamically sample a Gaussian distribution of reaction barrier heights depending on their state, molecular orientation, and impact parameter within the surface unit cell [55–57]. According to this interpretation, $\bar{E}_d(\upsilon)$ corresponds to the mean dynamical barrier to dissociation which Mortensen et al. [30] calls the "adiabatic barrier." Unfortunately, the nonlinear equation (6) is relatively insensitive to the choice of parameters and reasonable fits to experimental eigenstate-resolved dissociative sticking coefficients

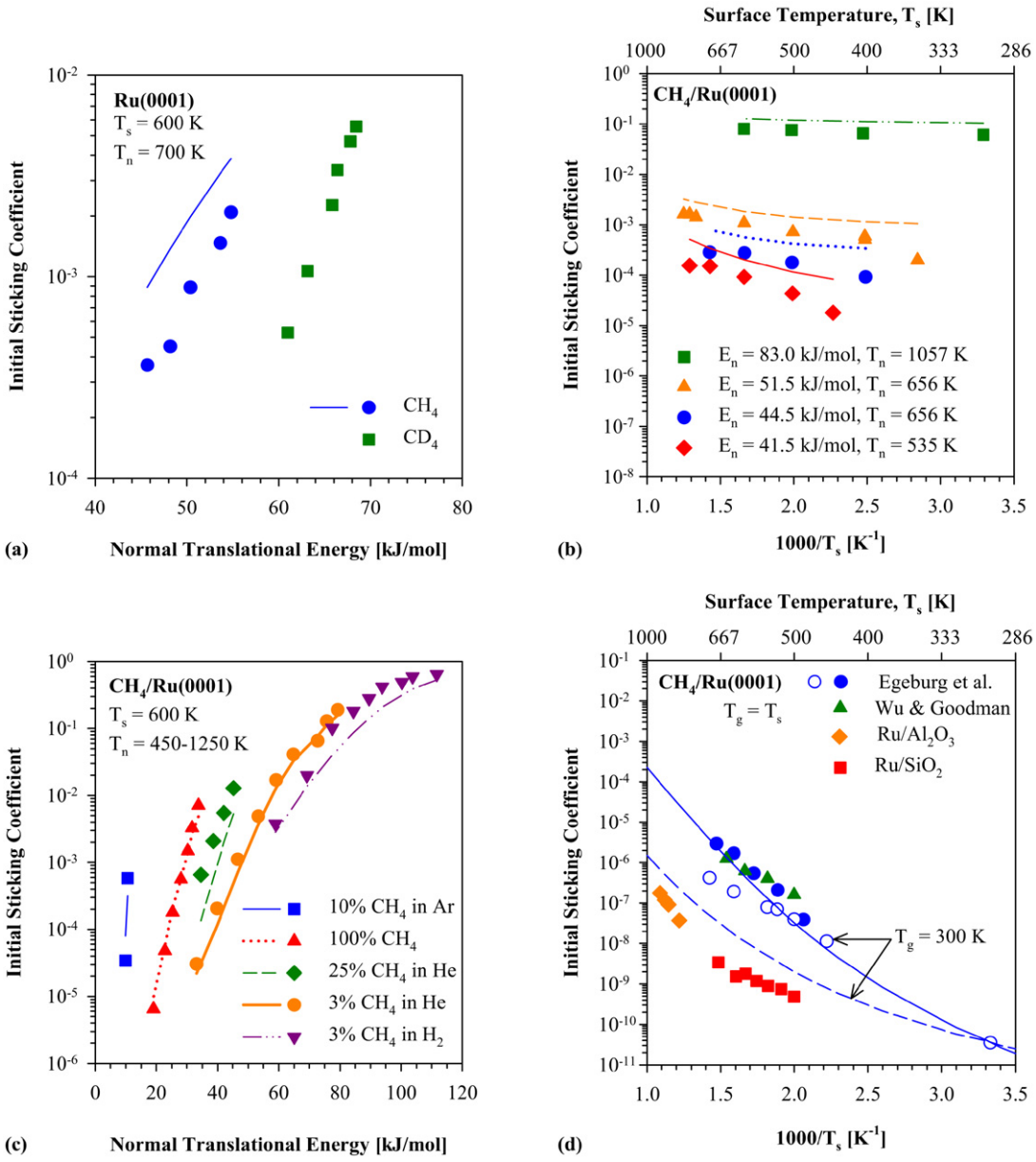

Fig. 4. Dissociative sticking coefficients, S, for methane on Ru(0001) derived from experiments (points) are compared to semiempirical error function model simulations (lines) using Table 1 parameters. The overall ARD is 208%. Supersonic molecular beam derived [30] S as a function of: (a) E_n yields an ARD for the CH_4 data of 136%; (b) T_s yields an ARD = 145%; (c) E_n and T_n for various seeding mixtures at $T_s = 600$ K yields an ARD = 92%, slightly worse than the original T_s-independent parameter set specified by Larsen et al. [29] (i.e., $W(v = 0) = 27$ kJ/mol) which gave an ARD = 75%. (d) Thermal bulb derived S_T for ambient CH_4 gas randomly impinging on Ru(0001) [27,28] and Ru nanocatalyst [3,32] surfaces. Open points and dashed lines are for $S(T_s; T_g = 300$ K). The ARD for the Ru(0001) thermal bulb data is 532%.

can be obtained with quite different $\bar{E}_d(v)$ values, as illustrated in Fig. 8 of [9].

Fig. 4 shows the same experimental data presented in Fig. 2 with simulations based on the erf fitted model. Dissociative sticking curves were calculated by averaging the erf $S_v(E_n)$ over the normal translational and vibrational energy distributions for CH_4, assuming that methane is a pseudodiatomic molecule with an intramolecular "C–H stretching" vibration at 2925 cm^{-1} with vibrational quanta of 34.99 kJ/mol. Rotational energy was assumed to be a spectator to the dissociation dynamics, and only the $v = 0$, 1, 2 vibrational states were considered in the erf simulations [29,30]. The nine parameters required to generate the erf fitted dissociative sticking curves of Fig. 4 are listed in Table 1. (Note that $A(v) = 1$ was assumed, and so only the remaining six parameters were optimized to fit the dissociative sticking coefficients.) These parameters were originally reported by Larsen et al. [29], and Mortensen et al. [30] later included a surface temperature dependence in $W(v = 0, T_s)$. Although it uses several times more adjustable parameters than the PC–MURT, the erf model is able to achieve somewhat better overall agreement with the CH_4/Ru(0001) dissociative sticking experiments (cf. erf model ARD = 208% vs PC–MURT ARD = 316%). No erf model parameters have been experimentally determined for simulating

Table 1
Erf parameters used to simulate experimental dissociative sticking coefficients for CH_4 on Ru(0001) [29,30]

v	$\bar{E}_d(v)$ (kJ/mol)	$W(v, T_s)$ (kJ/mol)	$A(v)$
0	115	$19 + 0.014T_s$	1
1	65	14	1
2	16	0.001	1

the CD_4/Ru(0001) dissociative sticking of Fig. 4a, and there is no theoretical prescription for deriving the necessary parameters from the existing CH_4/Ru(0001) parameters.

3.3. Reaction dynamics

It is of interest to ascertain the relative importance of different molecular and surface degrees of freedom in promoting dissociative chemisorption. Chorkendorff et al. [27,29] have discussed the role of molecular vibrational excitation in the thermal dissociative sticking of CH_4 under the assumptions of the pseudodiatomic model in which $v = 0$, 1, and 2 vibrational states obeyed the erf functional sticking form. The incremental contribution to the thermal sticking coefficient from the ν_3 asymmetric C–H stretching vibration with $v = 0$, 1, and 2 quanta of excitation can also be calculated using PC–MURT according to

$$\delta S_v = P_{\nu_3} \int_{E_{\nu_3}}^{\infty} S(E^*) f_{\text{oth}}(E^* - E_{\nu_3})\, dE^*, \tag{7}$$

where P_{ν_3} is the Maxwell–Boltzmann probability for having a particular ν_3 vibrational state at energy E_{ν_3}, $S(E^*)$ is the microcanonical sticking coefficient, and $f_{\text{oth}}(E^* - E_{\nu_3})$ is the convolved initial energy distribution for all active degrees of freedom of the molecule and surface other than the ν_3 vibration of CH_4. Table 2 compares the contribution of each vibrational eigenstate to the total thermal sticking S_T as determined by the erf model and PC–MURT. Both models indicate that molecules in the ν_3 ground state will dominate the thermal dissociative sticking at low temperature. However, the erf model predicts that vibrationally excited molecules with $v = 2$ will dominate the thermal sticking at $T \geqslant 800$ K and that the successfully reacting molecules will be characterized by a vibrational population inversion. A vibrational efficacy is sometimes defined as [30,58]

$$\xi_v = \frac{\bar{E}_d(v-1) - \bar{E}_d(v)}{E_v(v) - E_v(v-1)} = \frac{\Delta \bar{E}_d}{\Delta E_v} \tag{8}$$

to help characterize the effectiveness of vibrational energy in decreasing the normal translational energy requirement to surmount the mean dynamical barrier. A value of $\xi_v = 0$ indicates that vibrational energy does not enhance reactivity, whereas $\xi_v = 1$ indicates that vibrational energy is as effective as normal translational energy in promoting reaction, which is the hallmark of statistical theories such as PC–MURT. According to Table 1 erf parameters, the CH_4/Ru(0001) vibrational efficacies are $\xi_{v=1} = 1.43$ and $\xi_{v=2} = 1.40$, such that vibrational energy is ~40% more efficacious than normal translational energy in promoting reaction. The Polanyi rules [59] would argue that such a dynamical bias is consistent with a late transition state for dissociative chemisorption, but the reduced dimensionality erf model actually is too heavily averaged in interpreting the CH_4/Ru(0001) experiments to draw such an inference [30].

Table 2
Vibrationally-resolved contributions to the thermal dissociative sticking coefficient (i.e., $\delta S_v / S_T$) for CH_4 on Ru(0001)

T (K)	PC–MURT (%)			Erf model (%)		
	$v = 0$	$v = 1$	$v = 2$	$v = 0$	$v = 1$	$v = 2$
300	92.34	7.64	0.02	99.76	0.23	0.01
400	90.32	9.60	0.08	95.37	3.16	1.47
500	88.00	11.77	0.23	78.22	10.08	11.70
600	85.43	14.08	0.49	56.94	15.80	27.26
700	82.69	16.41	0.89	42.88	18.64	38.48
800	79.84	18.70	1.42	34.11	20.38	45.51
900	76.95	20.87	2.09	28.90	21.57	49.52
1000	74.08	22.87	2.86	25.68	22.53	51.79
1100	71.28	24.68	3.72	23.57	23.38	53.04
1200	68.57	26.29	4.65	22.33	24.10	53.57
1300	65.97	27.70	5.61	21.29	24.83	53.88

PC–MURT analysis of the role of different molecular vibrations in the thermal dissociative sticking of CH_4 on Ni(100) [9] indicates that sticking derived from the low-frequency, high-degeneracy ν_4-bending mode of methane contributes most to S_T over the temperature range $T = 300$–1000 K. Summing the sticking contributions from over 1400 vibrational states is necessary to account for just 95% of the thermal dissociative sticking for CH_4 on Ni(100) at $T = 1000$ K [9]. Consequently, the erf model cannot be practically implemented to calculate S_T for CH_4 by experimental consideration of all of the relevant vibrational states. In contrast to the erf model, PC–MURT requires optimization of just three reactive transition state parameters to simulate any equilibrium, nonequilibrium, or quantum-state resolved S through Eq. (2). This relative simplicity comes at the price that statistical transition state behavior is assumed even though mode-specific behavior has been observed in the dissociative chemisorption of methane on Ni(100) [13,15,16], Ni(111) [14], and Pt(111) [19] for some rovibrational quantum states. Current evidence suggests that such mode-specific behavior tends to average out toward the statistical limit when integrated over many quantum states, such as in calculations of thermal and nonequilibrium dissociative sticking coefficients for CH_4 on Ni(100) [8,9,43], Ir(111) [44], and Pt(111) [20]. Indeed, much of the activated dissociative chemisorption and recombinative desorption dynamics of H_2 on Cu(111) can be quantitatively reproduced [47] on the basis of the statistical transition state assumptions, even though molecular vibrational energy is only half as efficacious as normal translational energy in promoting dissociative chemisorption [58] for this benchmark system for gas-surface reaction dynamics.

PC–MURT provides a way to calculate the relative importance of the different molecular and surface degrees of freedom in supplying the energy necessary to overcome the reaction threshold energy, E_0. Fractional energy uptakes are defined as $f_i = \langle E_i \rangle_R / \langle E^* \rangle_R$, where $\langle E_i \rangle_R$ is the mean energy derived

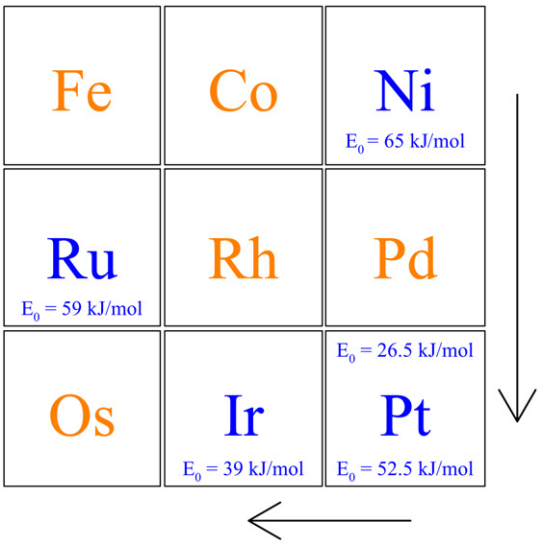

Fig. 5. PC–MURT predicted C–H bond activation energies based on low index single crystal surfaces are shown above (C_2H_6) and below (CH_4) the element abbreviation for a selection of transition metals ([8,20,44,45] and this work). Arrows indicate the observed trend in the apparent reaction threshold energy E_0 for CH_4 dissociation which decreases from top to bottom along and group and from right to left along a period (i.e., E_0 for Ni(100) > E_0 for Ru(0001) > E_0 for Pt(111) > E_0 for Ir(111)).

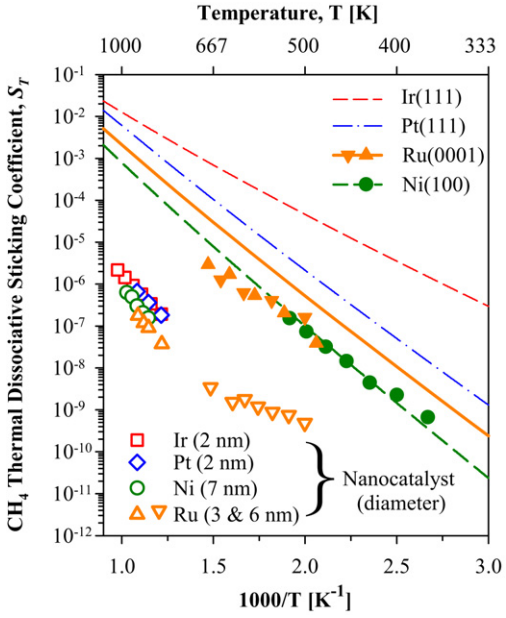

Fig. 6. Thermal dissociative sticking coefficients for CH_4 on transition metal nanocatalysts (open points) [1,3–6] derived from CH_4 decomposition rates are compared with PC–MURT simulations based on analysis of supersonic molecular beam experiments on single crystal surfaces (lines) ([8,20,44] and this work). Dissociative sticking coefficients for single crystal surfaces determined in thermal equilibrium bulb experiments are also shown where available (solid points) [27,28,60].

from a particular degree of freedom i for the successfully reacting PCs and $\langle E^* \rangle_R$ is the total mean energy for the successfully reacting PCs. For thermal dissociative chemisorption of CH_4 on Ru(0001) at $T = 600$ K, calculated fractional energy uptakes are $f_v = 41\%$, $f_s = 24\%$, $f_r = 21\%$, and $f_n = 14\%$ for the vibrational, surface phonon, rotational, and normal translational degrees of freedom, respectively. Molecular vibration contributes the preponderance of energy necessary to overcome E_0 under thermal equilibrium conditions, and normal translational energy contributes the least. Although supersonic molecular beam results of the kind illustrated in Fig. 2c draw particular attention to the near-exponential increase of S with increasing E_n, the PC–MURT model argues that independently increasing any form of the active exchangeable energy E^* in the PCs would have the same effect on S. Consequently, the relative importance of different forms of molecular and surface energy on the S_T is determined by the relative *availability* of energy from the different degrees of freedom at temperature T.

3.4. Catalysis versus surface science thermal dissociative sticking

PC–MURT has been applied to the activated dissociative chemisorption of several alkanes on single crystal transition metal surfaces [8,9,20,41–45] with generally better agreement with experiment than for CH_4 dissociation on Ru(0001) (e.g., ARD < 50% for CH_4/Ni(100) [8,43] vs ARD > 300% for CH_4/Ru(0001)). Fig. 5 shows a section of the periodic table with reaction threshold energies E_0 for cleaving the first C–H bond in C_2H_6 (shown above the element abbreviation) and CH_4 (shown below the element abbreviation) that were extracted from PC–MURT analysis of molecular beam and thermal bulb experiments. For CH_4 dissociative chemisorption, E_0 decreases down the group from nickel to platinum and left across the period from platinum to iridium. Without sufficient experimental data and PC–MURT analysis for rhodium and palladium surfaces, it is not yet clear whether the trend arrows shown in Fig. 5 should be straight or curved (i.e., will Ir and Rh have lower E_0 values than Os and Ru, respectively?).

The PC–MURT affords an opportunity to close the "non-equilibrium gap" that can hinder comparisons between non-equilibrium surface science experiments and thermal hetero-

Table 3
Arrhenius parameters for thermal dissociative sticking of CH_4 on transition metal surfaces and nanocatalysts[a]

	Surface	S_0	E_a (kJ/mol)	S_T at 600 K
PC–MURT	Ir(111)	2.2	44	3.41×10^{-4}
	Pt(111)	10.4	63	3.25×10^{-5}
	Ru(0001)	4.8	66	8.85×10^{-6}
	Ni(100)	3.5	71	2.10×10^{-6}
Experiment	Ru(0001) [27,28]	1.4×10^{-4}	55	7.87×10^{-7}
	Ni(100) [60]	1.4×10^{-1}	60	8.32×10^{-7}
	Ir (2 nm) [5,6]	4.6×10^{-2}	85	1.92×10^{-9}
	Pt (2 nm) [1]	3.1×10^{-2}	80	3.54×10^{-9}
	Ni (7 nm) [4]	2.1×10^{-1}	103	2.36×10^{-10}
	Ru (3 nm) [3]	7.2×10^{-2}	99	1.84×10^{-10}
	Ru (6 nm) [32]	5.8×10^{-7}	29	1.78×10^{-9}
	Ru (3 and 6 nm) [3,32]	1.9×10^{-2}	50	2.32×10^{-9}

[a] Arrhenius fits of the PC–MURT simulations to $S_T = S_0 \exp(-E_a/k_B T)$ were performed over the temperature range $T = 300$–1000 K, while Arrhenius fits for the experimental data were performed over the temperature range of the experiments.

geneous catalysis experiments. Fig. 6 and Table 3 compare PC–MURT simulations of CH_4 thermal dissociative sticking coefficients based on previous analysis of supersonic molecular beam experiments [8,20,44] on several different metal surfaces with experimental S_T values derived from thermal bulb experiments [27,28,60] and thermal catalysis experiments on analogous supported metal nanocatalysts [1,3–6]. Important to note is that for Wei and Iglesia's high-temperature nanocatalyst studies [1–6], initial turnover rates for methane decomposition were the same as steady-state turnover rates for steam and dry reforming, which led those authors to conclude that the surface remained essentially bare of adsorbates during reforming. Wei and Iglesia's nanocatalyst turnover rate constants for methane decomposition were converted to thermal dissociative sticking coefficients according to [44]

$$S_T = kN_s\sqrt{2\pi m k_B T}, \tag{9}$$

where k is the reported turnover rate constant in $s^{-1}\,Pa^{-1}$ and N_s is the areal density of exposed metal atoms on the nanocatalyst estimated from its value on that material's closest packed facet (e.g., for Ni, $N_s = 1.9 \times 10^{19}$ m^{-2} for Ni(111)). Under the same thermal equilibrium conditions, PC–MURT predicts that Ir(111) is the most reactive transition metal surface with respect to methane dissociative chemisorption followed by Pt(111), then Ru(0001), and finally Ni(100). Contrastingly, Wei and Iglesia's thermal catalysis experiments [1] indicate that Pt nanocatalysts are the most active for methane dissociative chemisorption followed by Ir, Ni, and, finally, Ru nanocatalysts. When plotted againts Fig. 6 logarithmic S_T scale, differences in nanocatalyst reactivity with metal composition become almost indistinguishable, whereas PC–MURT predicts much more dramatic differences on the single-crystal surfaces based on analysis of supersonic molecular beam experiments.

Along with differences in periodic reactivity trends, thermal dissociative sticking coefficients derived from nanocatalyst turnover rates are two to four orders of magnitude *lower* than PC–MURT predictions and thermal bulb experiments for S_T on single-crystal surfaces. This finding may be surprising, because high-curvature nanocatalysts should expose more surface steps and higher index surface planes that are typically more reactive than flat, low-index metal surfaces [36,61]. Structure sensitivity has been shown for reforming on the nanocatalysts, where turnover rates can be increased by about a factor of 5 with increasing dispersion [1]. Structure sensitivity in alkane dissociative sticking coefficients also has been demonstrated on Pd single-crystal surfaces where surfaces with more step edges or low coordination sites have higher dissociative sticking coefficients [21]. However, recent supersonic molecular beam measurements by Campbell et al. [55] comparing the reactivity of CH_4 on 3-nm Pd nanoparticles supported on MgO(110) and on Pd(111) found that the Pd nanoparticles were no more than twice as reactive as Pd(111) at a CH_4 incident translational energy of 71 kJ/mol. Given that Pd nanoparticles and single crystals display fairly similar reactivity for stoichiometric CH_4 dissociative chemisorption, it seems likely that the discrepancy between the nanocatalyst and single-crystal reactivity in Fig. 6 derives from a rapid buildup of CH_4 decomposition products on the nanocatalyst surfaces. In that case, average turnover rates or S_T values reported on a per initially exposed surface metal atom basis would be low compared with specific values for the relatively few active sites that remain available to turn over. For example, a rapid buildup of C could partially poison the surface, decreasing the apparent reactivity of the nanocatalysts. Such adsorbed or absorbed carbon atoms could change the local electronic structure of nearby surface metal atoms, reduce the nanocatalyst reactivity by site blocking, or limit the availability of ensembles of contiguous metal atoms necessary for methane dissociation. Wei and Iglesia [3] found that CO oxidation experiments performed before and after their high-temperature CH_4-reforming experiments exhibit the same CO oxidation rates. They concluded that the number of exposed metal atoms remains constant during reforming and that very little unreactive C is deposited. Unfortunately, it is not clear whether the time resolution of Wei and Iglesia's oxidation/reforming/oxidation switching experiments was such that transient oxidation of adsorbed C left behind from reforming would be readily identifiable.

Wei and Iglesia's [1–6] high-temperature methane reforming rates depend linearly on the pressure of CH_4 and are independent of co-reactant CO_2 or H_2O pressures over a considerable range. The first C–H bond cleavage of CH_4 is the rate-determining step in reforming under Wei and Iglesia's kinetic assumptions that all steps in the complete decomposition of methane to give surface-bound carbon and desorbing hydrogen gas are irreversible and that the surface is primarily bare under reactive conditions. However, more complicated reforming kinetics have been proposed [62–64], and the primarily bare surface assumption may be oversimplified [64] because much of the surface may rapidly accumulate carbon [4]. For example, in the first second of Wei and Iglesia's CH_4 decomposition experiments at 873 K and 250 mbar pressure of CH_4, there are roughly 4×10^7 collisions per exposed surface atom on the nanocatalysts and $S_T = 5 \times 10^{-4}$ on the Ru(0001) facets according to the PC–MURT. Consequently, at times below the time resolution of the catalysis experiments, it is likely that the nanocatalyst surface will be almost completely covered by methane decomposition products, presumably C at this high temperature. After a comparable 120-s exposure of 6.6 mbar of CH_4 on Ru(0001) at $T_s < 700$ K, Wu and Goodman [65] identified methylidyne (CH) and vinylidene (CCH_2) using post-exposure HREELS in UHV. Increasing the temperature beyond 800 K in UHV decomposed these hydrocarbon fragments and left only C on the surface. HREELS and CO titration TPD spectra were consistent with this C aggregating into a denser graphitic form, which left some of the Ru(0001) metal atoms reexposed. Consequently, Fig. 6 differences in CH_4 S_T values between single-crystal and nanocatalyst surfaces likely derives from the substantially reduced number of bare surface sites available for CH_4 decomposition on the nanocatalysts under the high-pressure, high-temperature conditions relevant to reforming (i.e., only $\sim 10^{-2}$–10^{-4} of the initially exposed metal atoms on the surface remain bare). More speculatively, the ~100 kJ/mol activation energy and similar rates for the high-temperature decomposition of CH_4 on the different metal

nanocatalysts suggest that the energetics of the submonolayer C motions necessary to expose reactive ensembles of surface metal atoms may dominate the CH_4 decomposition and reforming kinetics. Precise determination of exactly why the steady-state nanocatalyst reactivity substantially lags the stoichiometric reactivity observed for methane on the low-index single-crystal surfaces will require additional incisive experiments. Optimistically, however, this report suggests that it may be possible to enhance nanocatalyst reforming rates by as much as two to four orders of magnitude.

4. Conclusion

In this work, we used PC–MURT, a "local hot spot" model of gas-surface reactivity, to semiquantitatively reproduce dissociative sticking coefficients for methane on Ru(0001) derived from nonequilibrium supersonic molecular beam and thermal bulb experiments. PC–MURT analysis of methane molecular beam experiments indicated that the reaction threshold energy E_0 for the initial C–H bond cleavage of CH_4 decreased from 65 kJ/mol on Ni(100) [8,9], to 59 kJ/mol on Ru(0001) (this work), to 52.5 ± 2.5 kJ/mol on Pt(111) [20], to 39 kJ/mol on Ir(111) [44]. The relative importance of different molecular and surface degrees of freedom in supplying the energy necessary to overcome the activation barrier for CH_4 dissociation on Ru(0001) was assessed and compared with the predictions from an earlier erf dynamical model. Comparison between experimental and PC–MURT simulated thermal dissociative sticking coefficients S_T for methane on low-index metal surfaces with S_T values derived from methane decomposition rates on the analogous metal nanocatalysts suggests that there may be substantial opportunity to improve the performance of reforming catalysts.

Acknowledgments

This material is based on work supported by the National Science Foundation under CHE-0415540, CHE-0718657 and by the donors of the American Chemical Society Petroleum Research Fund.

References

[1] J.M. Wei, E. Iglesia, J. Phys. Chem. B 108 (2004) 4094.
[2] J.M. Wei, E. Iglesia, J. Catal. 225 (2004) 116.
[3] J.M. Wei, E. Iglesia, J. Phys. Chem. B 108 (2004) 7253.
[4] J.M. Wei, E. Iglesia, J. Catal. 224 (2004) 370.
[5] J.M. Wei, E. Iglesia, PCCP 6 (2004) 3754.
[6] J.M. Wei, E. Iglesia, Angew. Chem. 43 (2004) 3685.
[7] X.G. Zhang, R. Liyanage, P.B. Armentrout, J. Am. Chem. Soc. 123 (2001) 5563.
[8] H.L. Abbott, A. Bukoski, D.F. Kavulak, I. Harrison, J. Chem. Phys. 119 (2003) 6407.
[9] H.L. Abbott, A. Bukoski, I. Harrison, J. Chem. Phys. 121 (2004) 3792.
[10] P.M. Holmblad, J. Wambach, I. Chorkendorff, J. Chem. Phys. 102 (1995) 8255.
[11] L.B.F. Juurlink, P.R. McCabe, R.R. Smith, C.L. DiCologero, A.L. Utz, Phys. Rev. Lett. 83 (1999) 868.
[12] M.P. Schmid, P. Maroni, R.D. Beck, T.R. Rizzo, J. Chem. Phys. 117 (2002) 8603.
[13] R.D. Beck, P. Maroni, D.C. Papageorgopoulos, T.T. Dang, M.P. Schmid, T.R. Rizzo, Science 302 (2003) 98.
[14] R.R. Smith, D.R. Killelea, D.F. DelSesto, A.L. Utz, Science 304 (2004) 992.
[15] L.B.F. Juurlink, R.R. Smith, D.R. Killelea, A.L. Utz, Phys. Rev. Lett. 94 (2005) 208303.
[16] P. Maroni, D.C. Papageorgopoulos, M. Sacchi, T.T. Dang, R.D. Beck, T.R. Rizzo, Phys. Rev. Lett. 94 (2005) 246104.
[17] A.C. Luntz, D.S. Bethune, J. Chem. Phys. 90 (1989) 1274.
[18] J. Harris, J. Simon, A.C. Luntz, C.B. Mullins, C.T. Rettner, Phys. Rev. Lett. 67 (1991) 652.
[19] J. Higgins, A. Conjusteau, G. Scoles, S.L. Bernasek, J. Chem. Phys. 114 (2001) 5277.
[20] K.M. DeWitt, L. Valadez, H.L. Abbott, K.W. Kolasinski, I. Harrison, J. Phys. Chem. B 110 (2006) 6705.
[21] K. Klier, J.S. Hess, R.G. Herman, J. Chem. Phys. 107 (1997) 4033.
[22] S.L. Tait, Z. Dohnalek, C.T. Campbell, B.D. Kay, Surf. Sci. 591 (2005) 90.
[23] D.C. Seets, C.T. Reeves, B.A. Ferguson, M.C. Wheeler, C.B. Mullins, J. Chem. Phys. 107 (1997) 10229.
[24] T.A. Jachimowski, C.J. Hagedorn, W.H. Weinberg, Surf. Sci. 393 (1997) 126.
[25] S.G. Brass, G. Ehrlich, Surf. Sci. 187 (1987) 21.
[26] S.G. Brass, G. Ehrlich, J. Chem. Phys. 87 (1987) 4285.
[27] R.C. Egeberg, S. Ullmann, I. Alstrup, C.B. Mullins, I. Chorkendorff, Surf. Sci. 497 (2002) 183.
[28] M.-C. Wu, D.W. Goodman, Surf. Sci. 306 (1994) L529.
[29] J.H. Larsen, P.M. Holmblad, I. Chorkendorff, J. Chem. Phys. 110 (1999) 2637.
[30] H. Mortensen, L. Diekhoner, A. Baurichter, A.C. Luntz, J. Chem. Phys. 116 (2002) 5781.
[31] J.H. Larsen, I. Chorkendorff, Surf. Sci. Rep. 35 (1999) 165.
[32] J.N. Carstens, A.T. Bell, J. Catal. 161 (1996) 423.
[33] S. Dahl, A. Logadottir, R.C. Egeberg, J.H. Larsen, I. Chorkendorff, E. Tornqvist, J.K. Norskov, Phys. Rev. Lett. 83 (1999) 1814.
[34] S. Dahl, E. Tornqvist, I. Chorkendorff, J. Catal. 192 (2000) 381.
[35] I.M. Ciobica, F. Frechard, R.A. van Santen, A.W. Kleyn, J. Hafner, J. Phys. Chem. B 104 (2000) 3364.
[36] Z.P. Liu, P. Hu, J. Am. Chem. Soc. 125 (2003) 1958.
[37] Y.Z. Lin, J. Sun, J. Yi, J.D. Lin, H.B. Chen, D.W. Liao, J. Mol. Struct. Theochem. 587 (2002) 63.
[38] C.T. Au, C.F. Ng, M.S. Liao, J. Catal. 185 (1999) 12.
[39] I. Chorkendorff, J.W. Niemantsverdriet, Concepts of Modern Catalysis and Kinetics, Wiley–VCH, Weinheim, 2003.
[40] S.G. Wang, X.Y. Liao, J. Hu, D.B. Cao, Y.W. Li, J.G. Wang, H.J. Jiao, Surf. Sci. 601 (2007) 1271.
[41] A. Bukoski, D. Blumling, I. Harrison, J. Chem. Phys. 118 (2003) 843.
[42] A. Bukoski, H.L. Abbott, I. Harrison, J. Chem. Phys. 123 (2005) 094707.
[43] A. Bukoski, I. Harrison, J. Chem. Phys. 118 (2003) 9762.
[44] H.L. Abbott, I. Harrison, J. Phys. Chem. B 109 (2005) 10371.
[45] K.M. DeWitt, L. Valadez, H.L. Abbott, K.W. Kolasinski, I. Harrison, J. Phys. Chem. B 110 (2006) 6714.
[46] H.L. Abbott, I. Harrison, J. Chem. Phys. 125 (2006) 024704.
[47] H.L. Abbott, I. Harrison, J. Phys. Chem. A 111 (2007) 9871.
[48] H.L. Abbott, I. Harrison, J. Phys. Chem. C 111 (2007) 13137.
[49] D.F. Kavulak, H.L. Abbott, I. Harrison, J. Phys. Chem. B 109 (2005) 685.
[50] K.A. Holbrook, M.J. Pilling, S.H. Robertson, Unimolecular Reactions, Wiley, Chichester, UK, 1996.
[51] W. Forst, Unimolecular Reactions: A Concise Introduction, Cambridge Univ. Press, Cambridge, UK, 2003.
[52] H.F. Winters, J. Chem. Phys. 64 (1976) 3495.
[53] I.M. Ciobica, G.J. Kramer, Q. Ge, M. Neurock, R.A. van Santen, J. Catal. 212 (2002) 136.
[54] A.C. Luntz, J. Chem. Phys. 113 (2000) 6901.
[55] M. Balooch, M.J. Cardillo, D.R. Miller, R.E. Stickney, Surf. Sci. 46 (1974) 358.
[56] C.T. Rettner, L.A. Delouise, D.J. Auerbach, J. Chem. Phys. 85 (1986) 1131.

[57] H.A. Michelsen, D.J. Auerbach, J. Chem. Phys. 94 (1991) 7502.
[58] C.T. Rettner, H.A. Michelsen, D.J. Auerbach, J. Chem. Phys. 102 (1995) 4625.
[59] J.C. Polanyi, W.H. Wong, J. Chem. Phys. 51 (1969) 1439.
[60] B.O. Nielsen, A.C. Luntz, P.M. Holmblad, I. Chorkendorff, Catal. Lett. 32 (1995) 15.
[61] J. Rostrup-Nielsen, J.K. Norskov, Top. Catal. 40 (2006) 45.
[62] M.C.J. Bradford, M.A. Vannice, J. Catal. 183 (1999) 69.
[63] M.C.J. Bradford, M.A. Vannice, Catal. Rev. Sci. Eng. 41 (1999) 1.
[64] R.M. Rioux, A.L. Marsh, J.S. Gaughan, G.A. Somorjai, Catal. Today 123 (2007) 265.
[65] M.C. Wu, D.W. Goodman, J. Am. Chem. Soc. 116 (1994) 1364.